Comparative Study of the Electrochemical Behaviors for LiCoO$_2$ Electrode Coated with Two Different Al$_2$O$_3$ Coating Layer

Daxian Zuo, Guanglei Tian, Da Chen**, Kangying Shu*

College of Material Science and Engineering, China Jiliang University, Hangzhou, 310018, Zhejiang, China.
*E-mail: tianguanglei@cjlu.edu.cn, dchen_80@hotmail.com

The two samples of coated LiCoO$_2$ electrode with different microstructures of Al$_2$O$_3$ coating layer are prepared. The XRD, SEM and TEM results reveal that both Al$_2$O$_3$ coating layers attached on the surface of LiCoO$_2$ have different uniformity, thickness, morphology and crystallinity. The charge-discharge cycling results show different initial discharge capacity and cycle ability for both Al$_2$O$_3$-coated LiCoO$_2$ samples. The reasons causing electrochemical performance difference are ascribed to some following aspects: the different microstructure of both Al$_2$O$_3$ coating layer poses to the distinct interface resistance, which may lead to the different transport ability of Li ions as well as electrons through Al$_2$O$_3$ coating layer. And meantime, the electrolyte penetration to the Al$_2$O$_3$ coating is also different, which pose to different side reaction on the interface between cathode and electrolyte for both samples.

1. INTRODUCTION

Since LiCoO$_2$ was reported by J. B. Goodenough in 1980 [1], it has become a popular cathode material in the lithium ion secondary battery field, and due to its high capacity and compacted density, it has been widely investigated [2]. Although it has a high theoretical specific capacity of 274 mAh g^{-1} when entire lithium ions are extracted, its practical reversible capacity cannot be up to more than 140 mAh g^{-1} because of the side reactions between electrode and electrolyte and cobalt dissolution into electrolytes upon cycling [3-5]. Besides, it is well known that the interfacial resistance between LiCoO$_2$ electrode and electrolyte increases significantly and leads to the rapid capacity fade when the battery is cycled at a voltage over 4.2 V (vs. Li/Li$^+$) [6,7]. To decrease the capacity fade of LiCoO$_2$

during charge-discharge process above 4.2 V, many approaches has been developed. And one is to modify the cathode surface by coating $LiCoO_2$ particles with different metal oxides such as Al_2O_3 [8], TiO_2 [9], Fe_2O_3 [10], ZnO [11], CeO_2 [12], and ZrO_2 [13] etc., which has been recognized as one of the effective techniques among these different approaches for (i) lowering interfacial resistance between $LiCoO_2$ and electrolyte, (ii) reducing Co dissolution of $LiCoO_2$ into an electrolyte, and (iii) repression of mutual reaction between $LiCoO_2$ and electrolyte. Therefore, a good capacity retention is achieved by oxide coatings on $LiCoO_2$ even with a high upper limit voltage over 4.2 V (vs. Li/Li^+).

There are many literatures about alumina coating on $LiCoO_2$ [14-16], and as seen from these literatures, alumina coating can improve the electrochemical performance of $LiCoO_2$ to a certain extent. However, although these literatures use the same alumina coating, the electrochemical behavior of $LiCoO_2$ is quite different. Besides, the microstructure of alumina coating layer may be of great importance for enhancing the electrochemical properties of cathode material, and appropriate alumina coating layer could better diminish interface resistance and accelerate the transfer of electron and Li^+ ion. Unfortunately, so far, the influence of the microstructure of alumina coating layer on cathode electrochemical performance has rarely been studied. In the existing commercial cathode material, $LiCoO_2$ generally has a smooth surface and single crystal particle with 5-10 μm, and the continuity and uniformity of coating layer on the surface of $LiCoO_2$ are relatively good, which is beneficial to study the microstructure of alumina coating layer. Therefore, this paper takes $LiCoO_2$ with a large single crystal particle as cathode material and commercial coated alumina as coating material, prepares two different microstructures of Al_2O_3 coating layer, and studies the relationship between the microstructure of coating layer and the electrochemical behavior of cathode material.

2. EXPERIMENTAL

2.1. Sample preparation

2.1.1 Al_2O_3/$LiCoO_2$ I electrode

Commercial $LiCoO_2$ powders (Ningbo Jinhe New materials Co., Ltd, China), with an average particle size 5-10 μm, was regarded as pristine materials. Aluminum isopropoxide (AIP) was served as precursors, and we defined Al_2O_3-coated $LiCoO_2$ derived from AIP as Al_2O_3/$LiCoO_2$ I electrode. The weight ratios of $LiCoO_2$ to Al_2O_3 were 99.0:1.0. Typically, the stoichiometric amount of AIP firstly was dissolved in ethanol, and then the $LiCoO_2$ powders (29.7 g) and the polyvinyl pyrrolidone (PVP, 0.8 g)was added into the solution above. After that, the mixed solution was continuously stirred at 60 °C until the solvent was evaporated. Finally, the products were washed, dried and then treated at 600 °C for 4 hours, and the final samples were obtained.

2.1.2 Al_2O_3/$LiCoO_2$ II electrode

The pristine $LiCoO_2$ was the same as above-mentioned. Sodium metaaluminate (SMA) was served as precursors, and we defined Al_2O_3-coated $LiCoO_2$ derived from SMA as Al_2O_3/$LiCoO_2$ II

electrode. The weight ratios of $LiCoO_2$ to Al_2O_3 were 99.0:1.0. Typically, the $LiCoO_2$ powder (29.7 g) and polyvinyl pyrrolidone (PVP, 0.4 g) were homogeneously dispersed in 200 mL distilled water. Then the sulfosalicylic acid (0.3 g) as chelating agent was added into the mixed solution above. After the mixed solution above was stirred for 30 min at 50 °C, 0.06 M $NaAlO_2$ solution and 0.1 M CH_3COOH solution were pumped into the mixed solution above by peristaltic pump, respectively, meantime the solution pH value was adjusted to 10.0 by controlling pump speed. After the end of pumping process, the mixed solution above was sequentially stirred for 1 h at 50 °C. Finally, the products were filtered, washed, dried and then treated at 600 °C for 4 hours, and the final samples were gained.

2.1.3 Preparation of two different Al_2O_3 particles

The preparation process of Al_2O_3 particles was similar to the Experimental Section 2.1.1 and 2.1.2. For Al_2O_3 particles in the $Al_2O_3/LiCoO_2$ I electrode, the stoichiometric amount of AIP reagent was firstly dissolved in ethanol, and then the polyvinyl pyrrolidone (PVP, 0.8 g) was added into the solution above. After that, the mixed solution was continuously stirred at 60 °C until the solvent was evaporated. At last, the products were washed, dried and then treated at 600 °C for 4 hours, and the final samples were gained. For Al_2O_3 particles in the $Al_2O_3/LiCoO_2$ II electrode, the polyvinyl pyrrolidone (PVP, 0.4 g) were firstly dispersed in 200 mL distilled water. Then the sulfosalicylic acid (0.3 g) was added into the solution above. After the mixed solution above was stirred for 30 min at 50 °C, 0.06 M $NaAlO_2$ solution and 0.1 M CH_3COOH solution were pumped into the mixed solution above by peristaltic pump, respectively, meantime the solution pH value was adjusted to 10.0 by controlling pump speed. After the end of pumping process, the mixed solution above was sequentially stirred for 1 h at 50 °C. At last, the products were filtered, washed, dried and then treated at 600 °C for 4 hours, and the final samples were gained.

2.2. Structure and morphology characterizations

Structure analysis of the pristine and the Al_2O_3-coated $LiCoO_2$ was carried out by X-ray diffractometer (XRD) (Thermo ARL, X' TRA) equipped with a nickel-filtered Cu-Kα radiation source. Microstructures of the Al_2O_3-coated particles were examined by a scanning electron microscope (SEM, HITACHI SU8010) and transmission electron microscope (TEM, JEOL JEM 2100). The electron diffraction spectroscopy (EDS) mapping was measured to determine the element distribution together with SEM in large field of view. The cobalt dissolution measurement was performed by the inductively coupled plasma (ICP) (PerkinElmer Optima 7000Dv instrument).

2.3. Electrochemical characterizations

Characterization methods was similar to the Experimental Section 2.3 from our published paper [17]. Electrochemical properties of the products were measured using coin cells (CR2430). The working electrodes were prepared by casting the slurry consisting of 90 wt% of active material, 5 wt%

of acetylene black as conductive additive, and 5 wt% of poly (vinylidene fluoride) (PVDF) (Alfa Aesar) as binding agent onto an aluminum foil. The electrolyte consisted of a solution of 1 M $LiPF_6$ in ethylene carbonate (EC)/dimethyl carbonate (DMC) (1:1, v/v). Lithium foil was used as counter electrodes. These cells were assembled in an argon-filled glovebox (Super 1220/750, MIKROUNA) and galvanostatically cycled between 3.0 V and 4.4~4.6 V (vs. Li/Li^+) on a multi-channel battery cycler (CT2001A, Wuhan LAND Electronic Co., Ltd). The electrochemical impedance spectroscopic (EIS) data were collected at an electrochemical workstation (CHI 660E, CH Instrumenets), with the frequency range set as 100 kHz to 10 mHz by applying an AC voltage of 5 mV amplitude. The cyclic voltammogram (CV) measurements were also carried out at room temperature on an Electrochemical Workstation (CHI 660E, CH Instrumenets) at a scan rate of 0.1 mV s^{-1} between 3.0 and 4.5 V (vs. Li/Li^+).

3. RESULTS AND DISCUSSION

3.1. Structure and morphology characterizations

The XRD patterns of $LiCoO_2$ coated with two different Al_2O_3 layers are compared with those of pristine $LiCoO_2$ in Fig. 1. The XRD patterns of all samples exhibit single-phase α-$NaFeO_2$ layered structure and are indexed assuming a hexagonal axes option of rhombohedral R-3m space group [18]. This suggests that the crystal structure of $LiCoO_2$ particles is hardly changed after Al_2O_3 coating. Besides, for the Al_2O_3-coated $LiCoO_2$ powders, there is no diffraction peaks corresponding to Al_2O_3 observed obviously in XRD patterns, which can be attribute to small amount of alumina existing on the surface of $LiCoO_2$ and may suggest that aluminum oxide acts as an amorphous thin film.
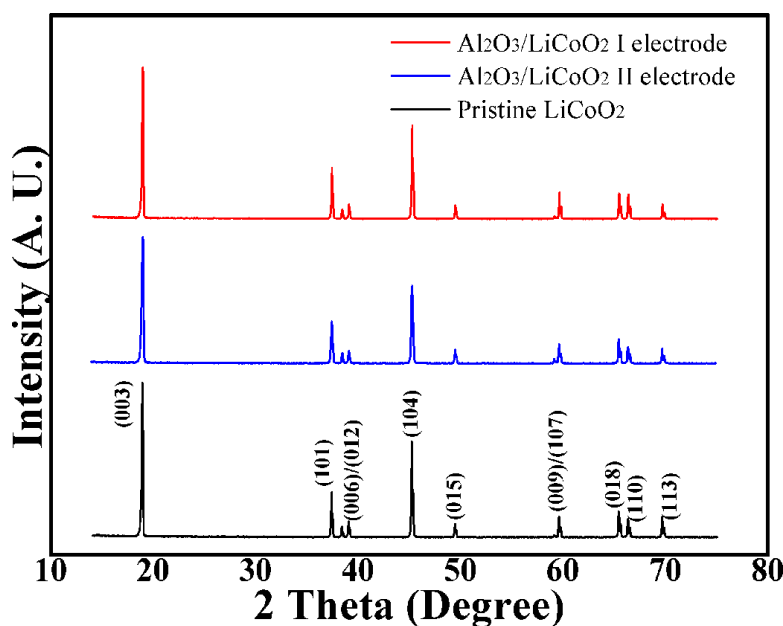

Figure 1. XRD patterns of the pristine $LiCoO_2$, $Al_2O_3/LiCoO_2$ I electrode and $Al_2O_3/LiCoO_2$ II electrode, respectively.
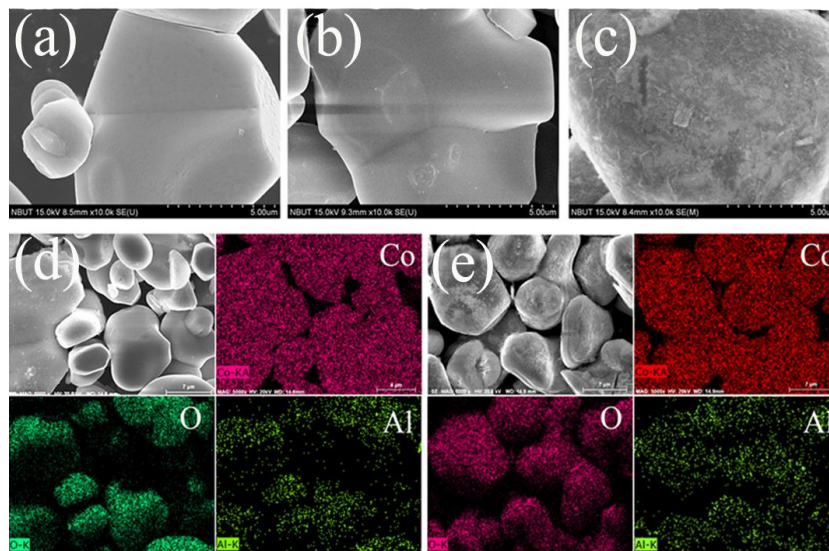
Figure 2. SEM images of (a) the pristine $LiCoO_2$, (b) $Al_2O_3/LiCoO_2$ I electrode, (c) $Al_2O_3/LiCoO_2$ II electrode. EDS dot-mappings for composition Co, O and Al of (d) $Al_2O_3/LiCoO_2$ I electrode, (e) $Al_2O_3/LiCoO_2$ II electrode, respectively.

The morphology of pristine and two different Al_2O_3-coated $LiCoO_2$ particle was characterized by SEM, and the images are shown in Fig. 2. As seen from Fig. 2a, obviously the surface of pristine $LiCoO_2$ is very smooth and seems rather "clean". In addition, for the two different Al_2O_3 coating, there is an obvious difference on the surface microstructure of coated $LiCoO_2$ electrode. As shown in Fig. 2b, the surface of $Al_2O_3/LiCoO_2$ I electrode reveals no distinguishable different compared with the pristine $LiCoO_2$, which is rather smooth and thus shows better uniformity. In comparison, Fig. 2c suggests that many small particles are attached on the surface of $LiCoO_2$, which show that this uneven and incomplete coating occurs on the surface of $Al_2O_3/LiCoO_2$ II electrode. These surface differences between both Al_2O_3 coatings may be posed by the different deposition environment of $Al(OH)_3$ such as pH value, Al^{3+} concentration and the properties of liquid phase [19]. Also, when the pH=10.0, the precipitation reaction of SMA is relatively rapid, thus a high local concentration is easily achieved on the $LiCoO_2$ surface. Contrarily, the hydrolysis rate of AIP is very slow, which could inhibit agglomeration of particles. Therefore, the Al_2O_3 coating layer for the $Al_2O_3/LiCoO_2$ I electrode is more compact and smoother than that of $Al_2O_3/LiCoO_2$ II electrode. In short, the SEM images reveal that the surface microstructure of both Al_2O_3 coating layer is greatly different, which may give rise to different electrochemical performances.

Fig. 2d and e presents the EDS mapping images of Co, O and Al in the $LiCoO_2$ particles coated by two different Al_2O_3 coating layers. Homogeneous distributions of Co, O and Al were observed in the coated $LiCoO_2$ electrode material. It is also seen that Al components are almost encapsulated on the whole surface and Al elements are dispersed in the most area of both samples, which prove that both Al_2O_3 coating layers are successfully attached upon the $LiCoO_2$ surface.
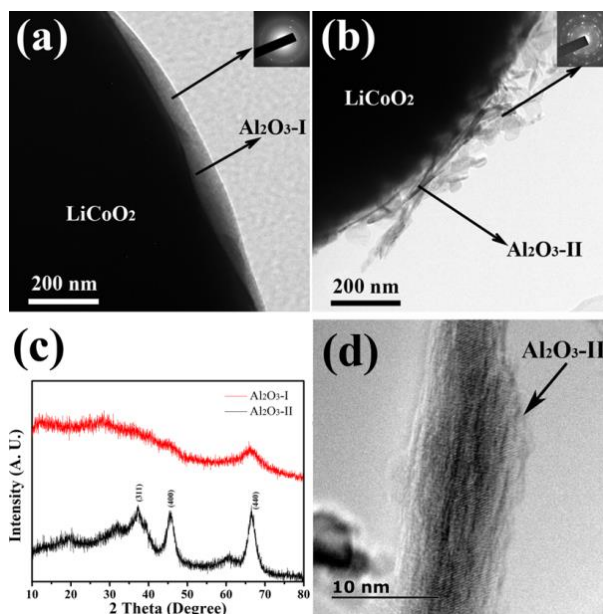
Figure 3. TEM images of (a) Al_2O_3/$LiCoO_2$ I electrode, (b) Al_2O_3/$LiCoO_2$ II electrode, respectively. (c) XRD patterns of both Al_2O_3. (d) High-resolution TEM images of Al_2O_3/$LiCoO_2$ II electrode.

To better analyze the microstructure difference between both Al_2O_3 coating layers, the TEM images of Al_2O_3/$LiCoO_2$ I and Al_2O_3/$LiCoO_2$ II electrode were examined, respectively. As shown in Fig. 3a, the magnified image around the edge of the surface-modified $LiCoO_2$ particle reveals that it is uniformly coated by a thin floc-like Al_2O_3 layer which has a thickness ranging from 20 to 50 nm. On the contrary, as seen from Fig. 3b, Al_2O_3/$LiCoO_2$ II electrode yields discontinuous deposition of Al_2O_3 coating layer, which makes the uniformity less than that of Al_2O_3/$LiCoO_2$ I electrode. Meantime, high-resolution TEM images of Al_2O_3/$LiCoO_2$ II electrode (Fig. 3d) suggests that this Al_2O_3-II coating layer is made of some thin Al_2O_3 sheets, which show different microstructure compared with Al_2O_3-I coating layer. Besides, the selected area electron diffraction (SAED) patterns of Al_2O_3 coating layer are definitely different between Al_2O_3/$LiCoO_2$ I electrode and Al_2O_3/$LiCoO_2$ II electrode. As shown in the right upper inset in Fig. 3a and b, the Al_2O_3 coating layer derived from Al_2O_3/$LiCoO_2$ I electrode shows completely amorphous, but as for the Al_2O_3/$LiCoO_2$ II electrode, the crystallization of Al_2O_3 coating layer is detected. Moreover, to further analyze the microstructure difference between both Al_2O_3 coating layers, the XRD patterns of two different Al_2O_3 particles are compared with each other in Fig. 3c. The preparation of the Al_2O_3 particles is shown in the Experimental Section 2.1.3. As seen from Fig. 3c, the XRD pattern of Al_2O_3 particles from Al_2O_3/$LiCoO_2$ I electrode is amorphous, which is consistent with SAED analysis. However, as for the Al_2O_3/$LiCoO_2$ II electrode, all the observed strong peaks of Al_2O_3 particles can be indexed to χ-Al_2O_3 (JPCD cards No. 50-0741), which present some crystallization of Al_2O_3. This significant difference founded in the microstructures of both Al_2O_3 coating layer imply that two Al_2O_3 coating layers may have the different properties of electron transfer and Li^+ diffusion ability, which can further result in the different electrochemical performance.
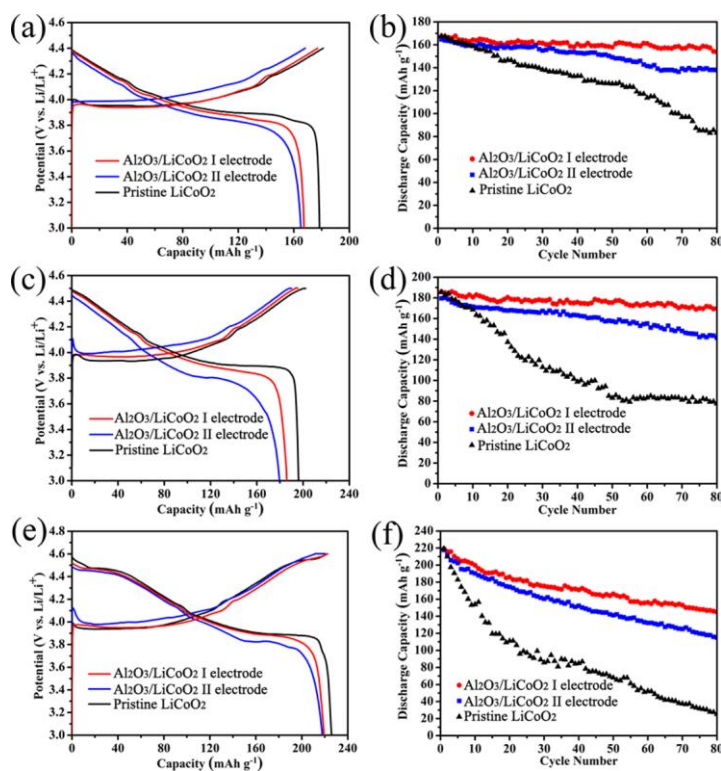
3.2. Electrochemical characteristics

Figure 4. The initial charge and discharge curves of pristine LiCoO$_2$, Al$_2$O$_3$/LiCoO$_2$ I electrode and Al$_2$O$_3$/LiCoO$_2$ II electrode in the voltage range of (a) 3.0-4.4 V, (c) 3.0-4.5 V and (e) 3.0-4.6 V at 0.1 C. The cycle performance curves of pristine LiCoO$_2$, Al$_2$O$_3$/LiCoO$_2$ I electrode and Al$_2$O$_3$/LiCoO$_2$ II electrode (b) between 3.0 and 4.4 V, (d) between 3.0 and 4.5 V, (f) between 3.0 and 4.6 V at 0.5 C.

The initial charge-discharge curves of the pristine and Al$_2$O$_3$-coated LiCoO$_2$ under the charging cutoff voltage 4.4, 4.5 and 4.6 V are shown in Fig. 4a, c and e, respectively. In comparison with the pristine one, the initial discharge capacity of Al$_2$O$_3$-coated samples is slightly decreased, regardless of Al$_2$O$_3$/LiCoO$_2$ I electrode or Al$_2$O$_3$/LiCoO$_2$ II electrode. The decreased capacities of the coated materials are attributed to the presence of the electro-inactive alumina and the diminution of amount of Co^{3+} available in the substituted surface oxide [20]. In addition, compared with Al$_2$O$_3$/LiCoO$_2$ II electrode, the initial discharge capacity of Al$_2$O$_3$/LiCoO$_2$ II electrode is slightly higher. This phenomenon may be explained that the resistance of Li ion migration or electron transfer in the both Al$_2$O$_3$ layer is different. Hence, when discharging Al$_2$O$_3$/LiCoO$_2$ II electrode, the sample will obtain larger polarization and result in a lower initial discharge capacity. Besides, as seen from Fig. 4b, d and f, after 80 cycles, the discharge capacity retention of pristine LiCoO$_2$ retains 49.7% in the voltage range from 3.0 to 4.4 V, 41.8% under the charging cutoff voltage 4.5 V, 13.6% under the charging cutoff voltage 4.6 V, respectively. However, compared to the pristine LiCoO$_2$, the Al$_2$O$_3$ coating effect becomes conspicuous after repeated charge-discharge cycling, and the discharge capacity retention of Al$_2$O$_3$-coated LiCoO$_2$ is enhanced largely. For example, for the Al$_2$O$_3$/LiCoO$_2$ I electrode, the discharge capacity retention is 91.8% under the charging cutoff voltage 4.4 V, 91.2% under the

charging cutoff voltage 4.5 V, 66.0% under the charging cutoff voltage 4.6 V, respectively. Besides, as for the Al_2O_3/$LiCoO_2$ II electrode, the corresponding discharge capacity retention is 83.7%, 80.0% and 52.8%, respectively. According to the TEM analysis above, both Al_2O_3 coating layers have different microstructure: the Al_2O_3-I coating layer is a thin floc-like amorphous, and the Al_2O_3-II coating layer presents some crystallization of sheet-like χ-Al_2O_3, which may cause different lithium ion diffusion and electron transfer [21], and thus lead to this cycle difference.
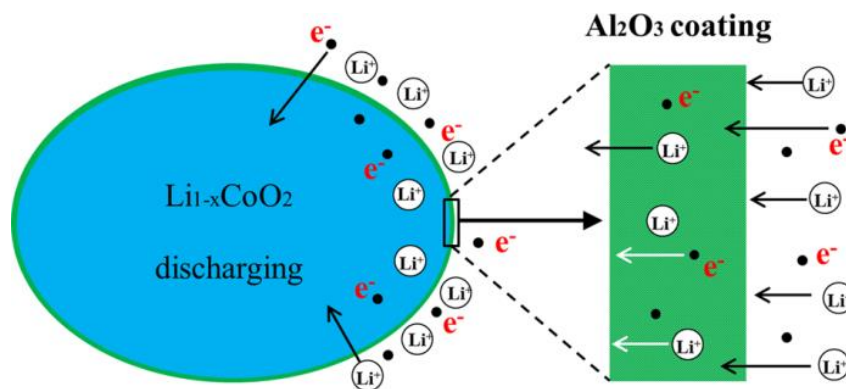

Figure 5. Schematic diagrams of the lithium ion diffusion and electron transfer through the surface of $LiCoO_2$.

As shown in Fig. 5, lithium ions and electrons through Al_2O_3 coating layer embed into the inner of $LiCoO_2$ during discharging, and different coating layers have different effects on the ability of Li^+ diffusion and electron transfer. For the Al_2O_3/$LiCoO_2$ I electrode, the floc-like amorphous microstructure may be more in favor of Li transport and electron transfer, meantime, the relatively short length scale of Al_2O_3 coating and better uniformity might aid faster lithium ion diffusion and electron transfer, which play an important role in electrochemical performance.

Table. 1 Electrochemical performances of $LiCoO_2$ electrode before and after coating by various oxides.

Cathode	Coating material	Electrochemical performance		Ref.
		Before coating (mAh g^{-1})	After coating (mAh g^{-1})	
$LiCoO_2$	Al_2O_3	0.5 C: 179.5 (initial); 49.7% (80 cycles)	0.5 C: 168.5 (initial); 91.8% (80 cycles)	This paper
$LiCoO_2$	Al_2O_3	0.2 C: 179.5 (initial); 59.0% (50 cycles)	0.2 C: 174.5 (initial); 97.5% (50 cycles)	[14]
$LiCoO_2$	Al_2O_3	0.2 C: 168.0 (initial); 80.0% (14 cycles)	0.2 C: 168.0 (initial); 80.0% (185 cycles)	[20]
$LiCoO_2$	ZnO	1.0 C: 178.0 (initial); 37.0% (30 cycles)	1.0 C: 179.0 (initial);65.0% (30 cycles)	[11]
$LiCoO_2$	ZnO	1.0 C: 174.8 (initial); 17.7% (30 cycles)	1.0 C: 171.5 (initial); 34.4% (30 cycles)	[22]
$LiCoO_2$	MgO	0.2 C: 150.0 (initial); 72.8% (60 cycles)	0.2 C: 156.0 (initial); 85.0% (60 cycles)	[18]
$LiCoO_2$	MgO	1.0 C: 178.5 (initial); 61.5% (100 cycles)	1.0 C: 188.5 (initial); 91.5% (100 cycles)	[23]

Table 1 lists some electrochemical performances of LiCoO$_2$ electrode before and after coating by various oxides for other earlier reports. As seen from it, when the LiCoO$_2$ electrode was coated by different coating materials, cathode electrochemical properties could behave with great differences, and even when the LiCoO$_2$ cathode material was coated by the same coating materials, the initial discharge capacity and cycle life also performed diverse. That is to say, the microstructure of coating layer and the properties of coating material play an important role in enhancing the electrochemical performance of cathode material. Moreover, because the transport abilities of Li$^+$ and electrons are the key factors to determine the battery performance, the Li$^+$ and electron transport properties of the coating layer directly affect the electrochemical performance of the coated material. Therefore, in order to obtain better electrochemical performance, the structure of coating material should be beneficial to Li$^+$ and electrons transportation, especially for the Li$^+$ ions.

To further analysis the reasons of capacity fade during cycling, the amount of cobalt dissolution was measured by inductively coupled plasma (ICP), which was correlated well with the capacity retention (Fig. 4). Moreover, the cobalt dissolution plays an important role in the ability of electrolyte penetration on the surface of LiCoO$_2$ electrode [24], and the stronger the cobalt dissolution into the electrolyte and side reactions on the interface is, the greater the extent of electrolyte penetration on the surface of LiCoO$_2$ is. As seen from Table 2, the amount of Co dissolution for the pristine LiCoO$_2$ electrode is about 2.031 mg L^{-1} at 4.4 V, and as the charge cutoff voltage increases to 4.6 V, the Co dissolution largely increases up to about 3.476 mg L^{-1}.

Table. 2 The cobalt dissolution amount at different charge cutoff voltages for the pristine LiCoO$_2$, Al$_2$O$_3$/LiCoO$_2$ I electrode and Al$_2$O$_3$/LiCoO$_2$ II electrode.

Sample	Co content dissolved in electrolyte (mg L^{-1})		
	(4.4 V)	(4.5 V)	(4.6 V)
Pristine LiCoO$_2$	2.013	2.741	3.476
Al$_2$O$_3$/LiCoO$_2$ I electrode	0.674	1.371	2.583
Al$_2$O$_3$/LiCoO$_2$ II electrode	0.723	2.150	3.272

However, the Co dissolution amount of both Al$_2$O$_3$-coated LiCoO$_2$ electrodes is less than that of the pristine LiCoO$_2$. Especially for the Al$_2$O$_3$/LiCoO$_2$ I electrode, the amount of Co dissolution is only 0.674 mg L^{-1} at 4.4 V, and with the charge cutoff voltage increasing to 4.6 V, the Co dissolution amount increase to about 2.583 mg L^{-1}.

Fig. 6 shows the variation trend between Co dissolution and charge cutoff voltage, which suggests that the Co dissolution amount increase with increasing the charge cutoff voltage. In addition, the amount of Co dissolution derived from Al$_2$O$_3$/LiCoO$_2$ I electrode is lower than that from Al$_2$O$_3$/LiCoO$_2$ II electrode, which may be related to uniformity and integrity of Al$_2$O$_3$ coating layer. The Al$_2$O$_3$-I coating layer has better uniformity and integrity, so the uncoated or the weak coated area is less. Therefore, this coating layer could better reduce the direct contact area of the LiCoO$_2$ with electrolyte, thus better prevent cobalt dissolution in the electrolyte and further restraint the electrolyte penetration on the surface of LiCoO$_2$.
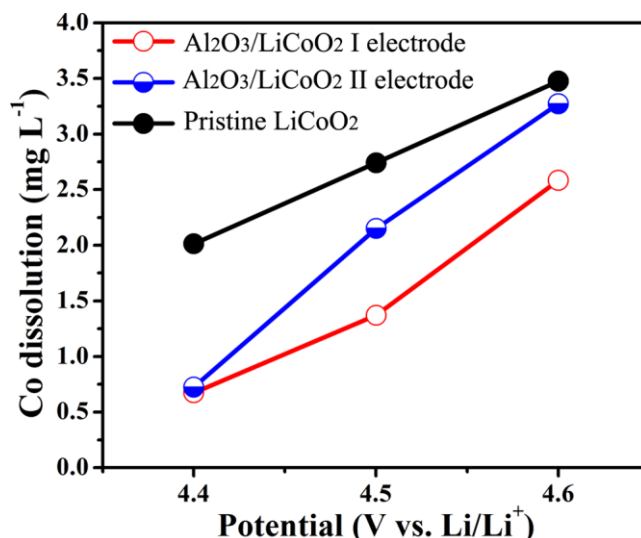
Figure 6. The relationship between cobalt dissolution and charge cutoff voltage for the pristine LiCoO$_2$, Al$_2$O$_3$/LiCoO$_2$ I electrode and Al$_2$O$_3$/LiCoO$_2$ II electrode.

Figure 7. Nyquist plots of the pristine LiCoO$_2$, Al$_2$O$_3$/LiCoO$_2$ I electrode and Al$_2$O$_3$/LiCoO$_2$ II electrode at a charge state of 4.4 V for (a) the 10th and (b) 40th cycle, (c) equivalent circuit performed to fit the Nyquist plot in (a) and (b). (d) Schematic diagrams of the interface change between the LiCoO$_2$ electrode and electrolyte in charging state.

In order to understand the effect of two Al$_2$O$_3$ coating layers on the AC impedance behavior of the Li/LiCoO$_2$ cells, AC impedance curves of the pristine LiCoO$_2$, Al$_2$O$_3$/LiCoO$_2$ I electrode and Al$_2$O$_3$/LiCoO$_2$ II electrode were measured at a charge state of 4.4 V after cycling. As shown in Fig. 7a and b, two distinct semicircles are observed. According to the previous AC impedance studies [25-27], the semicircle in the high frequency range can be attributed to the resistance due to Li$^+$ migration through the surface film on the electrode (R$_f$), while the semicircle observed in the high to medium frequency range is assigned to the charge transfer resistance between the electrode and electrolyte (R$_{ct}$).

The impedance parameters are calculated by the simplified equivalent circuit (Fig. 7c). As illustrated in Table 3, it can be seen that the R_f and R_{ct} increase dramatically during cycling for the pristine $LiCoO_2$, particularly, the R_{ct} is added up to about 6 times of the 10th value after 40 cycles. However, for the Al_2O_3-coated $LiCoO_2$ electrode, the R_f and R_{ct} increase very slowly, and the R_{ct} of the $Al_2O_3/LiCoO_2$ I electrode and $Al_2O_3/LiCoO_2$ II electrode only increases to about 1.2 and 1.8 times of the 10th value after 40 cycles, respectively. It reveals that both Al_2O_3 coating layers could effectively restrain the increase of interface resistance during cycling.

Table. 3 The impedance parameters of equipment circuits for the pristine $LiCoO_2$, $Al_2O_3/LiCoO_2$ I electrode and $Al_2O_3/LiCoO_2$ II electrode.

Samples	Pristine $LiCoO_2$		$Al_2O_3/LiCoO_2$ I electrode		$Al_2O_3/LiCoO_2$ II electrode	
	R_f	R_{ct}	R_f	R_{ct}	R_f	R_{ct}
After 10th	54.7	105.3	24.8	65.5	40.6	75.6
After 40th	294.4	610.5	31.2	81.5	59.5	140.6

Generally, there are some side reactions between the electrode surface and the electrolyte under the charged state shown in Fig. 7d, and with the cutoff voltage increasing, this interaction would be enhanced further [28, 29]. During the charge-discharge process, the electrolyte will decompose into Li_2CO_3/LiF and other products. And accompanied by the oxidation of electrolyte, there must be some Co^{4+} to be reduced to Co^{3+}/Co^{2+} [30].
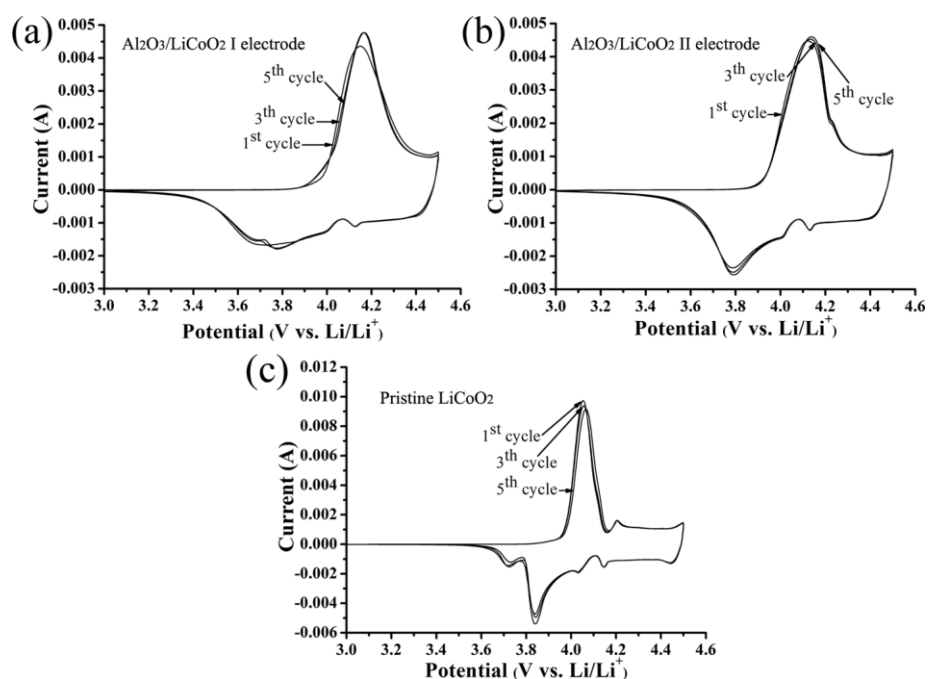

Figure 8. CV curves of the electrode materials of (a) $Al_2O_3/LiCoO_2$ I electrode, (b) $Al_2O_3/LiCoO_2$ II electrode and (c) the pristine $LiCoO_2$ from 3.0 to 4.5 V at a scan rate of 0.1 mV s^{-1}.

Fig. 7a and b shows that both surface film resistance and charge transfer resistance of the $Al_2O_3/LiCoO_2$ I electrode are lower than those of the $Al_2O_3/LiCoO_2$ II electrode. This supports the notion that the Al_2O_3 coating layer from $Al_2O_3/LiCoO_2$ I electrode could better decrease the side reaction between the electrode surface and the electrolyte under the charged state, and limit the growth of interface resistance due to the oxidative decomposition of electrolyte, which better improves the electrochemical performance of coated $LiCoO_2$ electrode.

Fig. 8 shows the cyclic voltammetry curve of the pristine $LiCoO_2$, $Al_2O_3/LiCoO_2$ I electrode and $Al_2O_3/LiCoO_2$ II electrode. As shown in Fig. 8c, the phase transition peaks is very clear and sharp. In addition, for the pristine $LiCoO_2$, all the curves have two strong oxidation peaks, a major oxidation peak at about 4.08 V and a minor one at 4.21 V, associated with their corresponding reduction peak at 3.83 V and 4.15 V, respectively, which can be attributed to the redox couple $Co^{3+}/^{4+}$ [31-33]. However, for the Al_2O_3-coated $LiCoO_2$ electrode, the phase transition peaks are smooth and obscure shown in Fig. 8a and b. And all the curves have only one strong oxidation peaks, a oxidation peak at about 4.17 V and corresponding reduction peak at 3.79 V. Furthermore, for the pristine $LiCoO_2$ electrode, due to some side reaction on the interface between electrolyte and electrode, the anodic peak potentials shift obviously in the first five cycles. Whereas with the sweeps going ahead, the curves of Al_2O_3-coated $LiCoO_2$ electrode are nearly identical, which may result from much different irreversible electrochemical reaction and phase transitions suppressed by Al_2O_3 coating layer, and thus indicate good reversibility. As a result, the cycle performance of coated $LiCoO_2$ electrode is improved progressively.

4. CONCLUSIONS

In this work, two different microstructures of Al_2O_3 coating layer are successfully prepared. Meanwhile, the relationship between the microstructure of Al_2O_3 coating layer and the electrochemical behaviors of coated $LiCoO_2$ electrode is investigated. The XRD, SEM and TEM results reveal that for the $Al_2O_3/LiCoO_2$ I electrode, an amorphous Al_2O_3 coating layer is found on the edge of the surface of $LiCoO_2$ with a thickness ranging from 20 to 50 nm, and furthermore, some sheet-like Al_2O_3 from the $Al_2O_3/LiCoO_2$ II electrode are attached on the surface of $LiCoO_2$ and its crystallization is detected. Besides, compared with the Al_2O_3-II coating layer, the Al_2O_3-I coating layer shows better uniformity and integrity, and the $Al_2O_3/LiCoO_2$ I electrode exhibits higher discharge capacity and better cycle stability. The reasons causing this performance difference are mainly ascribed to two aspects: on the one hand, due to different microstructure of both Al_2O_3 coating layer, the growth of the interface resistance during cycling performs different, which make the transport ability of Li ions as well as electrons through Al_2O_3 coating layer different; on the other hand, the electrolyte penetration ability on the surface of Al_2O_3-coated $LiCoO_2$ electrode is different, for the Al_2O_3-I coating layer, it can better reduce the direct contact area of the $LiCoO_2$ with electrolyte, and thus better prevent cobalt dissolution into the electrolyte and further restraint the electrolyte penetration.

References

1. K. Mizushima, P. C. Jones, P. J. Wiseman and J. B. Goodenough, *Mater. Res. Bull.*, 15 (1980) 783.
2. A. Aboulaich, K. Ouzaouit, H. Faqir, A. Kaddami, I. Benzakour and I. Akalay, *Mater. Res. Bull.*, 73 (2016) 362.
3. J. H. Shim, K. S. Lee, A. Missyul, J. Lee, B. Linn, E. C. Lee and S. Lee, *Chem. Mater.*, 27 (2015) 3273.
4. J. Tebbe, A. M. Holder and C. B. Musgrave, *ACS Appl. Mater. Inter.*, **7** (2015) 24265.
5. Y. Ito, Y. Sakurai, S. Yubuchi, A. Sakuda, A. Hayashi and M. Tatsumisago, *J. Electrochem. Soc.*, 162 (2015) A1610.
6. Y. Bai, K. Jiang, S. Sun, Q. Wu, X. Lu and N. Wan, *Electrochim. Acta*, 134 (2014) 347.
7. C. Huang, S. Zhuang and F. Tu, *J. Electrochem. Soc.*, 160 (2013) A376.
8. F. Zhao, Y. Tang, J. Wang, J. Tian, H. Ge and B. Wang, *Electrochim. Acta*, 174 (2015) 384.
9. S. Tian, L. L. Liu, Y. S. Zhu, Y. Y. Hou, C. L. Hu and Y. P. Wu, *Funct. Mater. Lett.*, 6 (2013) 1350016.
10. Q. Hao, C. X. Xu, S. Z. Jia and X. Y. Zhao, *Electrochim. Acta*, 113 (2013) 439.
11. W. Chang, J. W. Choi, J. C. Im and J. K. Lee, *J. Power Sources*, 195 (2010) 320.
12. H. W. Ha, N. J. Yun, M. H. Kim, M. H. Woo and K. Kim, *Electrochim. Acta*, 51 (2006) 3297.
13. D. Takamatsu, S. Mori, Y. Orikasa, T. Nakatsutsumi, Y. Koyama, H. Tanida, H. Arai, Y. Uchimoto and Z. Ogumi, *J. Electrochem. Soc.*, 160 (2013) A3054.
14. S. Oh, J. K. Lee, D. Byun, W. I. Cho and B. W. Cho, *J. Power Sources*, 132 (2004) 249.
15. H. M. Cheng, F. M. Wang, J. P. Chu, R. Santhanam, J. Rick and S. C. Lo, *J. Phys. Chem. C*, 116 (2012) 7629.
16. J. H. Woo, J. E. Trevey, A. S. Cavanagh, Y. S. Choi, S. C. Kim, S. M. George, K. H. Oh and S. H. Lee, *J. Electrochem. Soc.*, 159 (2012) A1120.
17. D. Zuo, G. Tian, D. Chen, H. Shen, C. Lv, K. Shu and Y. Zhou, *Electrochim. Acta*, 178 (2015) 447.
18. J. H. Shim, S. Lee and S. S. Park, *Chem. Mater.*, 26 (2014) 2537.
19. A. C. Dillon, A. W. Ott, J. D. Way and S. M. George, *Surf. Sci.*, 322 (1995) 230.
20. G. T. K. Fey, J. G. Chen and T. P. Kumar, *J. Power Sources*, 146 (2005) 250.
21. S. C. Jung and Y. K. Han, *J. Phys. Chem. Lett.*, 4 (2013) 2681.
22. S. M. Moon, W. Chang, D. Byun and J. K. Lee, *Curr. Appl. Phys.*, 10 (2010) e122.
23. N. Taguchi, T. Akita, K. Tatsumi and H. Sakaebe, *J. Power Sources*, 328 (2016) 161.
24. Z. Wang, X. Huang and L. Chen, *J. Electrochem. Soc.*, 151 (2004) A1641.
25. S. Y. Ye, H. K. Jin, S. Y. Lee, E. G. Shim and D. W. Kim, *J. Power Sources*, 196 (2011) 6750.
26. Y. Wang, H. Zhang, W. Chen, Z. Ma and Z. Li, *RSC Adv.*, 4 (2014) 37148.
27. J. Cao, G. Hu, Z. Peng, K. Du and Y. Cao, *J. Power Sources*, 281 (2015) 54.
28. Y. Orikasa, D. Takamatst, K. Yamamoto, Y. Koyama, S. Mori, T. Masese, T. Mori, T. Minato, H. Tanida, T. Uruga, Z. Ogumi and Y. Uchimoto, *Adv. Mater. Interfaces*, 1 (2014) 1400195.
29. D. Takamatsu, Y. Koyama, Y. Orikasa, S. Mori, T. Nakatsutsumi, T. Hirano, H. Tanida, H. Arai, Y. Uchimoto and Z. Ogumi, *Angew. Chem. Int. Ed.*, 51 (2012) 11597.
30. B. Han, D. Qian, M. Risch, H. Chen, M. Chi, Y. S. Meng and Y. S. Horn, *J. Phys. Chem. Lett.*, 6 (2015) 1357.
31. G. T. K. Fey, C. Z. Lu, T. P. Kumar and Y. C. Chang, *Surf. Coat. Tech.*, 199 (2005) 22.

32. C. Fu, G. Li, D. Luo, Q. Li, J. Fan and L. Li, *ACS Appl. Mater. Interfaces*, 6 (2014) 15822.
33. S. A. Needham, G. X. Wang, H. K. Liu, V. A. Drozd and R. S. Liu, *J. Power Sources*, 174 (2007) 828.